Applied Catalysis B: Environmental 168-169 (2015) 156–163

Contents lists available at ScienceDirect

Applied Catalysis B: Environmental

journal homepage: www.elsevier.com/locate/apcatb

Activity of PdO/SiO_2 catalysts for CH_4 oxidation following thermal treatments

Rahman Gholami, Kevin J. Smith*

Department of Chemical & Biological Engineering, University of British Columbia, 2360 East Mall, Vancouver BC V6T 1Z3, Canada

ARTICLE INFO

Article history:
Received 14 August 2014
Received in revised form
14 November 2014
Accepted 22 December 2014
Available online 24 December 2014

Keywords:
Natural gas vehicle
Emission control
Methane oxidation
Palladium catalyst
Hydrothermal aging
Catalyst sintering

ABSTRACT

The effect of thermal treatment of PdO/SiO_2 catalysts in air versus air/water at temperatures <973 K, is reported. PdO sinters during thermal aging in the presence of air (dry aging) and air/water (hydrothermal aging), but the growth and restructuring of the PdO crystallites is suppressed in the presence of added water, as observed in both continuous aging and cyclic aging experiments. The hydrothermally aged catalysts (PdO size ~3 nm) showed significantly lower CH_4 oxidation activity than the catalysts thermally aged in air (PdO size ~14 nm). A significant decrease in the Pd/Si ratio as measured by XPS, compared to a small growth in PdO size after hydrothermal aging, suggests PdO occlusion and hence a significant loss in activity following hydrothermal aging. The PdO occlusion and suppressed PdO particle sintering is attributed to SiO_2 overlayers on the PdO that are a consequence of hydroxyl mobility of the support, enhanced by the presence of added water.

1. Introduction

CH_4 has the highest H/C ratio among all hydrocarbon fuels and during combustion, generates the lowest amount of CO_2 per unit of energy [1–4]. These properties and the relatively low cost of natural gas, have led to a worldwide increase in the use of natural gas as a vehicle fuel. Natural gas vehicles (NGVs) release significant amounts of unburned CH_4 to the exhaust and since CH_4 is a greenhouse gas that has a global-warming potential 23x's that of CO_2, combustion of CH_4 is used to control the CH_4 emissions from NGVs [1,2,5]. However, the strength of the C—H bond in CH_4 (450 kJ/mol) relative to other hydrocarbons, and the low to moderate exhaust gas temperature of NGVs (423–873 K), means that controlling CH_4 emissions from NGVs is a major challenge [6].

Pd supported on various substrates is the most active metal for CH_4 oxidation [4,7–13]. C—H bond activation and interaction with lattice oxygen is reported to be the rate determining step in CH_4 oxidation [14]. Precise steady-state rate measurements on Pd single crystals at 600 K have confirmed bulk oxidation of Pd during reaction [15]. This indicates that PdO is the active phase, especially at the lower exhaust gas temperatures of NGVs where PdO is thermodynamically stable. However, morphological changes to the PdO and/or the support affect the Pd—O binding energy and contribute to the hysteresis effects observed during temperature-programmed CH_4 oxidation [3,4].

Despite a high initial activity, Pd catalysts deactivate after long periods of exposure to exhaust gas conditions [2,9]. The structural collapse of the catalyst support [7,16], sintering [17–19] and PdO→Pd conversion [7,8,20], have all been reported as contributors to catalyst deactivation during CH_4 oxidation. H_2O, present in the exhaust gas, also has an inhibitory effect on CH_4 oxidation [1,9,21–23] that is reversible and decreases with increased temperature [1]. Competitive adsorption between CH_4 and H_2O on the active sites of PdO has been suggested as the cause of catalyst inhibition [7,24]. Other reports suggest that in the presence of H_2O, PdO is converted to inactive $Pd(OH)_2$ [1] whereas Persson et al. [25] showed that water produced during reaction does not cause deactivation through physical restructuring of PdO. Schwartz et al. [23,26] used isotopic labeling combined with FTIR analysis to show that the accumulation of hydroxyls on the Pd catalyst surface impedes the oxygen exchange between the gas phase, PdO and the support and this limits catalyst activity.

In practice, catalysts are typically aged at high temperature (>1178 K) in the presence of water prior to assessment, to mimic aged catalyst performance [17,27,28]. At temperatures above about 1078 K, PdO decomposes to Pd [29] so that high temperature aging results in sintering of Pd^0 [17,27], a process that is influenced by the support [7,16] and enhanced in the presence of steam [17,27].

* Corresponding author. Tel.: +1 6048223601; fax: +1 6048226003.
E-mail address: kjs@mail.ubc.ca (K.J. Smith).

http://dx.doi.org/10.1016/j.apcatb.2014.12.037
0926-3373/

Table 1
Effect of thermal aging on the properties of 7.7 wt.% Pd/SiO_2.

Catalyst	Treatment	BET area m^2/g	Pd/Si[a] at%	Phase –	Cluster size XRD nm	Cluster size TEM nm	CO uptake[b] μmol/g
A	Reduced in H_2 at 673 K for 1 h	314	0.92	Pd	15 (1 1 1)	16 ± 11	62
B	Catalyst A heated in air at 723 K for 15 h	291	1.29	PdO	5 (1 0 1)	2 ± 1	174
C	Catalyst A heated in air at 873 K for 15 h	291	1.55	PdO	6 (1 0 1)	3 ± 1	160
D	Catalyst B air-aged at 973 K[c] for 16 h	268	1.31	PdO	23 (1 0 1)	14 ± 6	36
E	Catalyst B reduced in H_2 at 673 K for 1 h	304	0.82	Pd	7 (1 1 1)	8 ± 5	254
F	Catalyst B H_2O-aged at 973 K[d] for 16 h	274	0.98	PdO	11 (1 0 1)	3 ± 1	137

[a] Determined by XPS.
[b] CO chemisorption after reduction in H_2 at 100° C.
[c] Thermally aged at 973 K in 100 cm^{-3} min^{-1} STP of air for 16 h.
[d] Hydrothermally aged at 973 K in 100 cm^{-3} min^{-1} STP of 20 (v/v)% H_2O/air for 16 h.

The effect of hydrothermal aging at lower temperatures has also been reported. Escandón et al. [9] hydrothermally aged a Pd/ZrO_2 catalyst at 573–823 K prior to CH_4 combustion and reported an irreversible decrease in CH_4 conversion for the hydrothermally aged catalyst compared to the Pd/ZrO_2 that was not hydrothermally aged. More recently, Park et al. [30] compared a Pd/ZrO_2 and a Pd/Al_2O_3 catalyst, both hydrothermally aged at 873 K for 100 h. The Pd/ZrO_2 was more active and had higher stability than the Pd/Al_2O_3, illustrating the importance of support effects on the stability of PdO catalysts.

In the present study, we report on the effect of various thermal treatments on PdO/SiO_2 catalysts used for CH_4 oxidation. Catalyst aging in the presence of dry air versus wet air, at temperatures relevant to NGV applications (< 978 K) and below the PdO thermodynamic decomposition temperature, are compared. The loss in catalyst activity is discussed in terms of characterization data obtained before and after thermal aging.

2. Experimental

2.1. Catalyst preparation

Pd/SiO_2 catalysts with different Pd loadings were prepared using the procedure described by Sotoodeh and Smith [31]. Accordingly, SiO_2 (Sigma–Aldrich, 1.15 cm^3 g^{-1} pore volume, 60–200 mesh) was impregnated with a $PdCl_2$ (Sigma–Aldrich, 99% purity) solution, prepared by adding a few drops of 0.5 N HCl and heating to enhance dissolution. The impregnated catalysts were equilibrated for 48 h before being dried for 8 h at 393 K in ambient air. The dried sample was calcined in He (Praxair, UHP) for 6 h at 773 K following heat-up at a rate of 5 K min^{-1}, to ensure removal of residual Cl [31], then reduced in H_2 (Praxair, UHP) for 1 h at 673 K and finally cooled in He to room temperature (Catalyst A, Table 1). The reduced catalyst was further oxidized in situ in a flow of dry air (Praxair, Extra dry air) at 723 K for 15 h (Catalyst B, Table 1), following heat-up at a rate of 10 K min^{-1}, before activity assessment and characterization. Other thermal treatments of Catalyst A and B investigated in the present study are presented in Table 1.

2.2. Catalyst characterization

The BET surface area, pore volume, and pore size distribution of the catalysts was determined from the N_2 adsorption isotherms measured at 77 K using a Micromeritics ASAP 2020 analyzer. Samples were degassed for 4 h at 473 K in vacuum prior to analysis. The Barrett–Joyner–Halenda method applied to the desorption data was used to determine pore size. The CO uptake of the reduced catalysts (Pd/SiO_2) was measured using a Micromeritics AutoChem 2920 analyzer. The oxidized catalyst sample was purged in Ar at 373 K for 1 h to remove moisture, reduced in 10 (v/v)% H_2/Ar (Praxair, certified purity) at 373 K for 1 h, and then purged in He and cooled to 298 K. The CO uptake of the Pd was measured by passing pulses of CO at 298 K over the sample and measuring the CO adsorbed using a thermal conductivity detector (TCD). The AutoChem 2920 analyzer was also used to estimate the degree of Pd oxidation and verify the temperature at which Pd oxidation occurred. The dried SiO_2 impregnated with $PdCl_2$ was calcined in Ar (Praxair, UHP) for 6 h at 773 K following heat-up at 5 K min^{-1} from room temperature. After cooling to room temperature, the calcined catalyst was reduced in a 30 mL (STP) min^{-1} flow of 10 (v/v)% H_2/Ar for 1 h at 673 K following heat-up from room temperature at a rate of 10 K min^{-1}. After cooling to room temperature in He, the reduced sample was then oxidized in a 30 mL (STP) min^{-1} flow of 10 (v/v)% O_2/He (Praxair, certified purity) while heating at a rate of 10 K min^{-1} and monitoring the exit flow with a TCD. The oxidized sample was again cooled in He and re-oxidized at the same conditions to confirm that no further oxygen consumption occurred. The amount of O_2 consumed during the experiment was used to estimate PdO content after oxidation by assuming the reaction stoichiometry $2Pd + O_2 \rightarrow 2PdO$. Hence the degree of oxidation based on the total amount of Pd on the catalyst before temperature-programmed oxidation (TPO), was calculated.

X-ray diffraction patterns of the catalysts were collected using a Bruker D8 Focus (LynxEye detector) with CoKα1 radiation (λ = 1.79 Å) a 35-kV source, an angle scan range from 3° to 80° with a 0.04° step size and 0.8 s time steps. The crystallite size was estimated using the Scherrer equation. X-ray photoelectron spectroscopy (XPS) was carried out using a Leybold Max200 X-ray photoelectron spectrometer. Al Kα was used as the photon

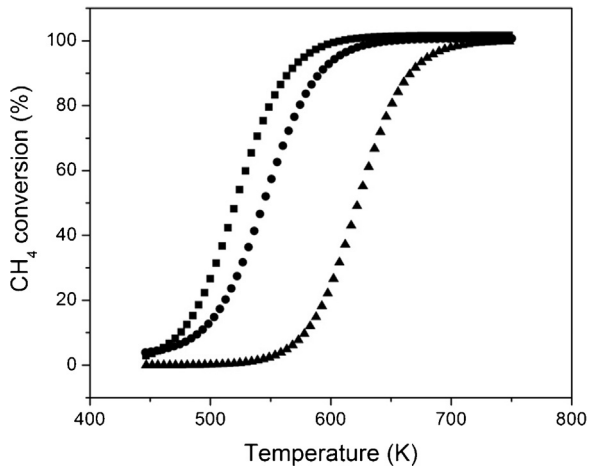

Fig. 1. Effect of thermal aging on 7.7 wt.% Pd/SiO_2 catalysts; (■) Catalyst B, (●) Catalyst D, (▲) Catalyst F; catalyst identity follows Table 1. TPMO condition: 1000 ppmv CH_4 and 20 (v/v)% O_2 in Ar and He, 5 K min^{-1}, GHSV 180,000 mL g^{-1} h^{-1}.

source generated at 15 kV and 20 mA. The pass energy was set at 192 eV for the survey scan and 48 eV for the narrow scan. The XPS spectra were corrected to the C1s peak at 285.0 eV. Transmission electron microscopy (TEM) images were obtained using a FEI Tecnai G2, 200 kV LaB_6 filament, with a 1.4 Å point-to-point resolution. The samples were ground in a pestle and mortar for a set period, dispersed in ethanol and sonicated for 5 min. A single drop of the dispersion was placed on a 300 mesh copper grid coated with Formvar-Carbon film before analysis. More than 150 clusters were counted and measured from the TEM images of each pre-treated sample and then fitted by a lognormal distribution to determine the average cluster size. Raman spectra were collected using a Ren-iShaw Invia Raman microscope and a 785 nm laser, with 10% laser power and 200 s acquisition time. Sample aggregates (~160 μm size) were analyzed at room temperature to identify PdO. The laser power and acquisition time were optimized to obtain the highest signal intensity for the PdO peak at ~650 nm. Raman spectra of the pure SiO_2 support were compared to the PdO/SiO_2 catalyst to identify PdO.

2.3. Reaction system and activity measurements

The experimental setup for catalyst testing consisted of a stainless steel, fixed-bed microreactor operated in plug flow (length: 5 cm; inside diameter: 0.9 cm) placed inside an electric tube furnace with a PID temperature controller. Two thermocouples (*K*-type), inserted inside the reactor, measured the temperature at the top and bottom of the catalyst bed. The catalyst (90–354 μm) was diluted four times (volume/volume) with inert SiC pellets to ensure isothermal operation. Feed flows were set using electric mass flow controllers (Brooks 5850 TR) and a liquid pump (Gilson 307), able to provide the desired flowrates of the feed gas components CH_4 (0.76 (v/v)% CH_4/Ar, Praxair, certified purity), O_2 (Praxair, UHP), H_2O (distilled and deionized), Ar (Praxair, UHP), He (Praxair, UHP) and air (Praxair, Extra dry air) for a total flowrate of 300 mL (STP) min^{-1}. The feed gas, typically 1000 ppmv CH_4 and 20 (v/v)% O_2 in inert gas and H_2O as required, were pre-heated to 373 K using a separate furnace before entering the reactor. Temperature-programmed CH_4 oxidation (TPMO) with 1000 ppmv CH_4, 20 (v/v)% O_2, and balance of He and Ar as the feed gas was used to evaluate the catalysts. Accordingly, the reactor temperature was ramped from ambient to 873 K at 5 K min^{-1}. The exit stream composition was continuously monitored using a quadrupole mass spectrometer (QMS; Thermo Scientific VG ProLab ThermoFisher Scientific Inc.). Subsequently, the CH_4 conversion as a function of temperature was determined to provide the initial activity of the catalyst for CH_4 oxidation. The stability of the catalysts was assessed by thermal aging of the catalysts in the reactor at different temperatures in a flow of air or 6.5 (v/v)% H_2O/air for 16 h before evaluation by TPMO.

3. Results

3.1. Catalyst aging in air and air/water

The effect of different thermal environments on the catalyst properties was investigated first. The reduced 7.7 wt.% Pd/SiO_2 catalyst (A) was calcined at 723 K (Catalyst B) or 873 K (Catalyst C) for 15 h in a 100 mL (STP) min^{-1} air flow and then cooled to room temperature in air. Subsequently, Catalyst B was thermally aged for a further 16 h in 100 mL (STP) min^{-1} of dry air at 973 K (Catalyst D), or hydrothermally aged in a 100 mL (STP) min^{-1} flow of 6.5 (v/v)% H_2O in air at the same temperature (973 K; Catalyst F). The activity of catalysts B, D, and F was evaluated by TPMO (Fig. 1). The data show that hydrothermal aging significantly deactivated the PdO/SiO_2 catalyst (F) when compared to thermal aging in dry air (D), as reflected in the shift in the light-off curves of the hydrothermally-aged sample towards higher temperature (Fig. 1). The $T_{50\%}$ (the temperature

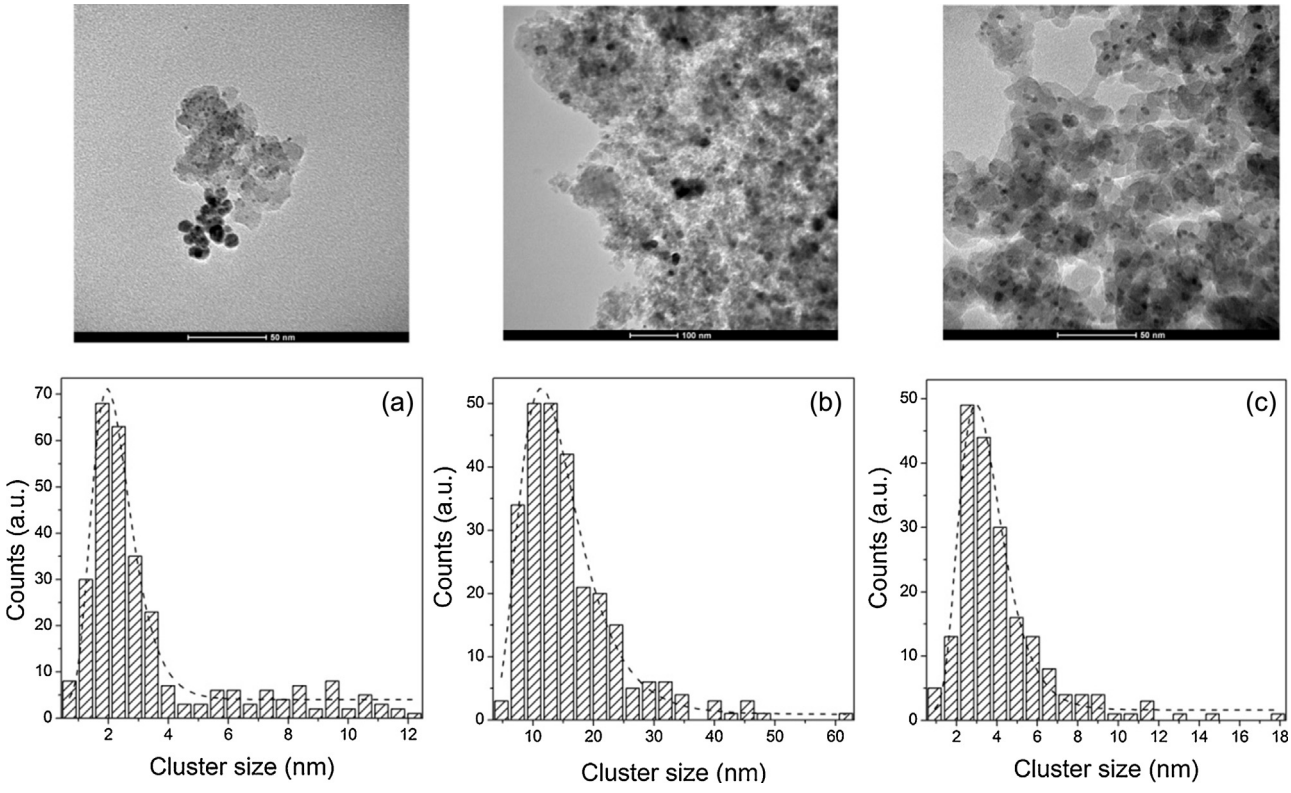

Fig. 2. TEM images and cluster size distributions of 7.7 wt.% Pd/SiO_2 catalysts (a): Catalyst B; (b): Catalyst D; and (c): Catalyst F. Catalyst identity follows Table 1.

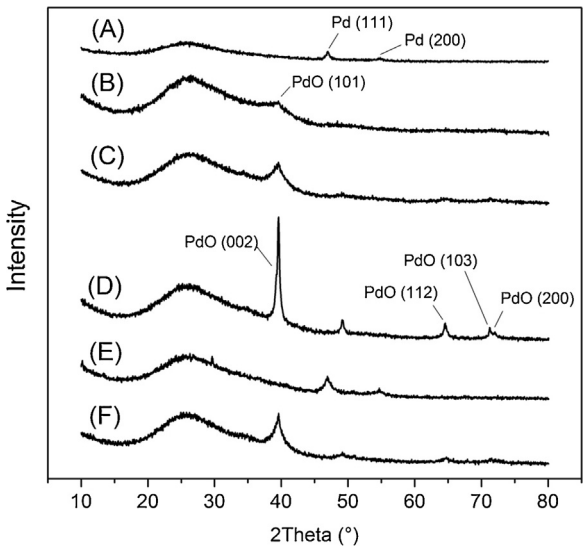

Fig. 3. XRD patterns of 7.7 wt.% Pd/SiO_2 catalyst following thermal treatments at the conditions described in Table 1. Catalyst identity follows Table 1.

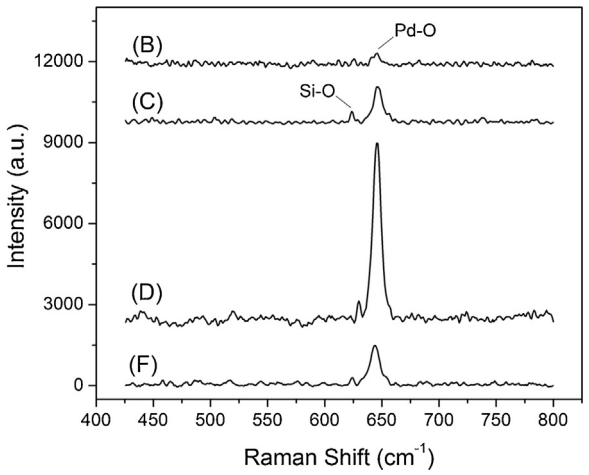

Fig. 4. Raman spectrums of 7.7 wt.% Pd/SiO_2 following thermal treatments as identified in Table 1.

at which 50% of the CH_4 had been converted) increased from 521 K for the calcined catalyst (B), to 544 K for the air-aged sample (D), compared to 623 K for the hydrothermally-aged sample (F).

Table 1 summarizes the properties of the 7.7 wt.% Pd/SiO_2 catalysts after the thermal treatments, showing significant differences in the properties after the thermal treatment in air versus air/water. The TEM analysis of the catalysts, summarized in Fig. 2, showed that the PdO TEM cluster size increased from 2.2 nm (Catalyst B) when the reduced Pd/SiO_2 (Catalyst A) was calcined at 723 K, to 3.2 nm when calcined in air at 873 K (Catalyst C). Aging in dry air at 973 K for a further 16 h (Catalyst D), yielded an average PdO cluster size of 13.5 nm, compared to 3.3 nm after aging in air/water at 973 K for a further 16 h (Catalyst F). These data show that calcination of the reduced Pd/SiO_2 (Pd cluster size ~16 nm), yields smaller PdO particles, that grow upon further thermal treatment in air or water, but the PdO growth rate is slower in water than in air. Furthermore, the data for Catalyst E show that reduction of the small PdO particles (Catalyst B) yields Pd particles about half the size of those present in the unused Pd/SiO_2 catalyst (Catalyst A) i.e., the thermal oxidation/reduction of the catalyst and the associated change in PdO/Pd size, is partly reversible. The data of Table 1 also show that the PdO/Pd cluster size data trends based on the TEM analysis are consistent with the XRD and CO chemisorption data.

The XRD patterns of Fig. 3 show that as the severity of the oxidation in air increased from 723 K for 15 h (Catalyst B) to an additional 16 h at 973 K (Catalyst D), there was less broadening of the PdO reflections (increased cluster size) and the intensity of the X-ray reflections increased. The transformation of Pd to PdO in the presence of air is known to be a relatively slow process, that is dependent upon temperature [7,32]. Consequently the changes in the XRD patterns likely reflect both increased conversion of Pd to PdO and growth of the PdO crystallites as the oxidation severity increased. The Raman spectra measured for selected catalysts (Fig. 4) are consistent with increased Pd to PdO conversion with increased oxidation severity. The peak at approximately 650 nm^{-1} in Fig. 4, present in all three samples (B, D, and F), corresponds to PdO [30,33,34]. Interpretation of the spectra is complicated by the fact that the PdO signal intensity is only proportional to the amount of PdO present for PdO crystallites <10 nm in size [33,35]. Nevertheless, the spectra clearly show that increased severity of the oxidation increased the amount of PdO on the catalyst, since the most intense signal was obtained for Catalyst D, which had the largest PdO clusters. Hence we conclude that increased oxidation severity results in both increased PdO cluster size and more complete conversion of Pd to crystalline PdO.

The Raman spectra of the hydrothermally aged catalyst (F), when compared to the air aged catalyst (D), also show that in the presence of water there was both less growth of the PdO crystallites and less conversion of Pd to PdO. The XRD data of Fig. 3 do not show the presence of Pd in the oxidised catalysts D or F, likely because of the low concentration of Pd in the sample and the disordered Pd/PdO_x structure that results after the oxidation at relatively low temperatures [35].

The oxidation of the Pd present in the reduced Catalyst A, to yield PdO, was further demonstrated by the XPS analysis of the 7.7 wt.% Pd/SiO_2 catalyst (Fig. 5). The XPS data show that after oxidation of Catalyst A at 723 and 873 K, PdO was present on the surface (Catalyst B and C), and re-reduction of this calcined sample, yielded Pd^0 (Catalyst E). The Pd/Si atom ratio, which can be taken as a measure

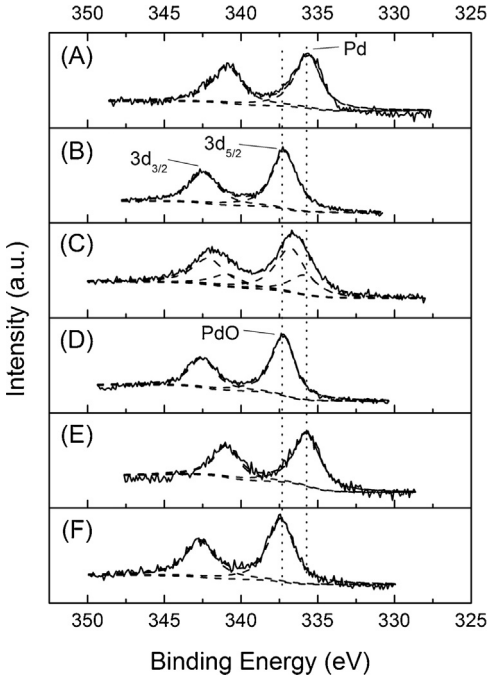

Fig. 5. XPS narrow scan spectra of 7.7 wt.% Pd/SiO_2 following thermal treatments as identified in Table 1.

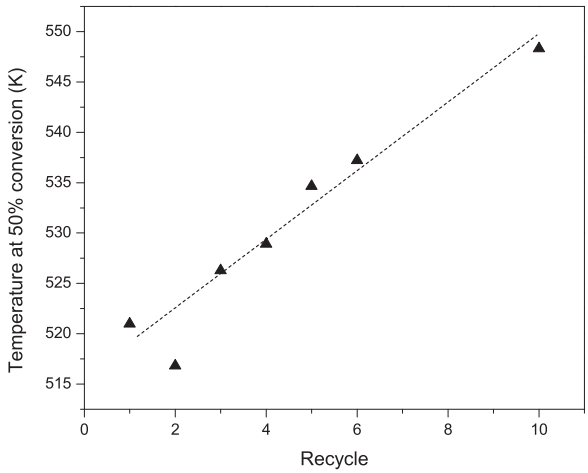

Fig. 6. The $T_{50\%}$ as a function of recycle number for the 7.7 wt.% Pd/SiO_2 catalyst with hydrothermal aging in 6.5% (v/v) H_2O/air at 973 K for 4 h after each TPMO; TPMO condition: 1000 ppmv CH_4 & 20% (v/v) O_2 in Ar & He, 5 K min^{-1}, GHSV 180,000 mL g^{-1} h^{-1}.

of Pd dispersion [36], increased after oxidation of Pd, corresponding to a reduced cluster size as observed from the TEM, XRD, and CO chemisorption data. The reduction of Catalyst B resulted in a decrease Pd/Si atomic ratio to 0.82. It is apparent that the oxidized samples have higher dispersion in comparison to the reduced samples.

Experiments in which the stability of the 7.7 wt.% Pd/SiO_2 catalyst was examined through repeated reaction and aging cycles were also completed. Catalyst B was examined by TPMO. Subsequently the catalyst was hydrothermally aged in a flow of 100 mL (STP) min^{-1} of 6.5 (v/v)% H_2O/air at 973 K for 4 h. The hydrothermally-aged sample was then cooled to 393 K in Ar and purged in Ar for 1 h. The TPMO and hydrothermal aging steps were subsequently repeated several times. The $T_{50\%}$ as a function of cycle number, reported in Fig. 6, increased from 521 K to 549 K after 10 cycles. After the 2nd cycle the extent of catalyst deactivation, reflected in the increase in the $T_{50\%}$ temperature at each cycle, was the same since the $T_{50\%}$ temperature increased linearly with cycle number. Note that the $T_{50\%}$ decreased after the 1st cycle, a consequence of previously reported PdO restructuring and hysteresis effects that are a result of the exposure of the catalyst to temperatures above the calcination temperature (723 K) during the first TPMO test [7,32]. Also note that the $T_{50\%}$ after four cycles, corresponding to a 16 h cumulative hydrothermal aging time, was 535 K, significantly lower than the $T_{50\%}$ of the hydrothermally-aged Catalyst F reported in Fig. 1 (623 K). Clearly, continuous aging for 16 h had more impact on the catalyst compared to the case where the catalyst was exposed to CH_4/O_2 at high temperature during TPMO between each of the four 4-h hydrothermal aging cycles. The sequential aging results show that the deactivation that occurs following exposure to air/water at high temperature is attenuated by the lower average partial pressure of H_2O that exists during sequential aging, compared to continuous aging.

3.2. Effect of Pd loading

The effect of hydrothermal aging on Pd/SiO_2 catalysts with different Pd loadings was also investigated. Catalysts with 0.6, 1.7, and 7.7 wt.% Pd supported on SiO_2 were hydrothermally aged at 973 K in 6.5 (v/v)% H_2O/air for 16 h and then evaluated by TPMO. Fig. 7 shows the activity results as a function of Pd loading. Note that an increase in Pd loading expectedly shifted the light-off curves towards lower temperatures because as the catalyst Pd loading increased, the mass

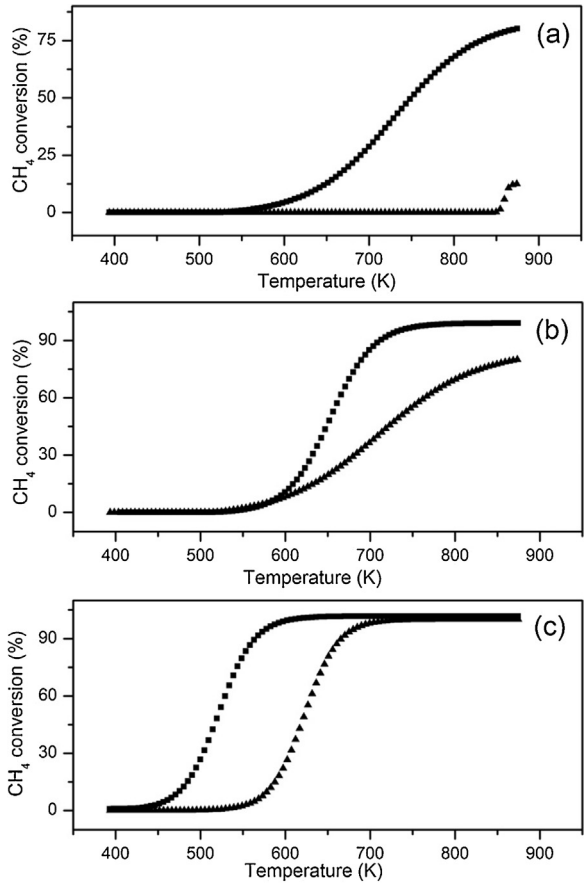

Fig. 7. Effect of hydrothermal aging on (a) 0.6, (b) 1.7, (c) 7.7 wt.% Pd/SiO_2 catalysts; (■) fresh sample, pre-oxidized in air at 723 K for 15 h; (▲) sample hydrothermally aged at 973 K in 6.5 (v/v)% H_2O/air for 16 h; TPMO condition: 1000 ppmv CH_4 & 20 (v/v)% O_2 in Ar & He, 5 K min^{-1}, GHSV 180,000 mL g^{-1} h^{-1}.

of Pd per unit volume of reactor also increased since the mass of catalyst was held constant for each experiment. Hydrothermal aging significantly deactivated the Pd-loaded catalysts, reflected in the considerable shift in light-off curves of the hydrothermally-aged catalysts toward higher temperatures (Fig. 7). The surface area of the calcined and hydrothermally-aged catalysts with different Pd loadings are summarized in Table 2. Although there was a decrease in surface area after hydrothermal aging, the pore size remained unchanged.

The effect of Pd loading on the deactivation observed during repeated hydrothermal aging and TPMO cycles was also investigated. For the 1.7 wt.% Pd/SiO_2, the $T_{50\%}$ after the 1st cycle (4 h hydrothermal aging) decreased from 643 K to 577 K, showing an increase in catalyst activity (Fig. 8). Further cycles show the expected catalyst deactivation, as observed for the 7.7 wt.% Pd/SiO_2

Table 2
Effect of hydrothermal aging on Pd/SiO_2 catalysts: pre-oxidized at 723 K in air 15 h (Fresh), aged at 973 K in 6.5 (v/v)% H_2O in air for 16 h (Aged).

		Surface area		Pore size		Pore volume	
Pd loading[a] wt%	CO uptake μmol/g_{Pd}	Fresh m^2 g^{-1}	Aged	Fresh nm	Aged	Fresh cm^3 g^{-1}	Aged
0[b]	–	310	266	11	11	1.1	1.0
0.6	500	344	282	10	10	1.1	0.9
1.7	2471	322	239	10	10	1.0	0.8
7.7	2260	291	274	11	10	1.0	0.9

[a] Pd/SiO_2; fresh, calcined He 773 K, Reduced H_2 673 K, then air, 723 K.
[b] SiO_2 support.

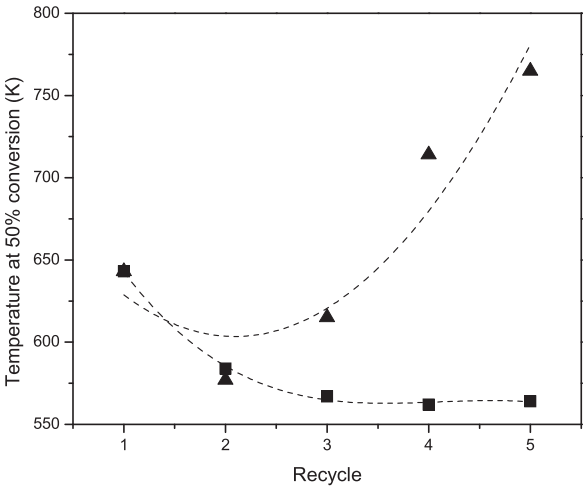

Fig. 8. The $T_{50\%}$ as a function of recycle number for the 1.7 wt.% Pd/SiO_2 catalyst: (■) thermally aged in air at 973 K for 4 h after each TPMO; (▲) hydrothermally aged in 6.5% (v/v) H_2O/air at 973 K for 4 h after each TPMO. TPMO condition: 1000 ppmv CH_4 & 20 (v/v)% O_2 in Ar & He, 5 K min^{-1}, GHSV 180,000 mL g^{-1} h^{-1}.

catalyst (Fig. 6). The $T_{50\%}$ increased from 577 K to 765 K after four cycles. To clarify whether an increase in the catalyst activity after the first 4 h hydrothermal aging cycle was a result of the added H_2O in the gas stream or not, the cycle of aging and activity measurements was carried out on the calcined 1.7 wt.% Pd/SiO_2 catalyst, but the catalyst was aged in dry air rather than air/water. Fig. 8 shows a sharp decrease in the $T_{50\%}$ temperature from 643 K to 584 K as observed in the previous experiment with H_2O (Fig. 6, after the 1st cycle) and then, the $T_{50\%}$ decreased further to 564 K (Fig. 8). If structural changes that occur during aging allow the PdO to restructure and crystallize, yielding a more active catalyst, as noted in the literature [7,32], then the data show again that restructuring of the catalyst in the presence of water is inhibited compared to that which occurs in a dry atmosphere.

4. Discussion

Previous studies have shown that the oxidation of Pd^0 occurs first through rapid uptake of a monolayer of O_2, followed by the formation of a sub-oxide (PdO_x) as Pd—O islands. Due to strong metal-support interactions, the islands tend to separate from each other and PdO re-dispersion occurs. The sub-oxide is slowly transformed to an active crystalline PdO phase [1,7,20,32,34,35,37,38]. Crystalline PdO is believed to form at approximately 775 K [7]. Complete oxidation of the Pd is therefore difficult and by TPO of Catalyst A (not shown), we estimated about 35% of the Pd was converted to PdO following the initial calcination in air at 723 K for 15 h. Similar data have been reported previously [32,34]. The data of Table 1 are consistent with the PdO nucleation mechanism described above. The PdO cluster size after calcination in air at 723 K was significantly smaller than the Pd cluster size, reflecting the re-dispersion of PdO. A further increase in temperature to 973 K sintered the PdO clusters and increased the Pd→PdO conversion (as shown by the Raman spectra). However, the data of Table 1 also show that hydrothermal aging inhibited the sintering of the PdO. Furthermore, the catalyst activity after both the continuous aging and cyclic aging experiments showed significant deactivation after hydrothermal aging.

Several studies have demonstrated the inhibition effect of water on PdO catalysts during CH_4 combustion [7,37,39,40]. The inhibition is strongly dependent on temperature, with inhibition less important at temperatures >723 K because of desorption [40]. Surface hydroxyls that interrupt O-exchange are thought to be the cause of the inhibition [23,26]. Studies in which water was added to the reactant gas have shown the inhibition to be reversible such that if the added water is removed, the catalyst activity returns to that observed prior to water addition [9,41]. On the other hand, when Pd catalysts are hydrothermally aged at elevated temperatures, they undergo significant, irreversible deactivation, as observed in the present study. Xu et al. [17] reported that the main deactivation mechanism of Pd/Al_2O_3 catalysts following exposure to 10 (v/v)% H_2O/N_2 at 1173 K for up to 200 h was due to Pd sintering. A substantial decrease in Pd dispersion from 3.71% to 0.86% over 7 wt.% Pd/Al_2O_3 and similar decrease over other Pd loadings after 96 h hydrothermal aging was observed. The BET surface area of the 7 wt.% Pd/Al_2O_3 catalyst was also reduced from 82.3 to 31.9 m^2 g^{-1} with aging time, attributed to Al_2O_3 phase transformations. As noted by Xu et al. [17], aging the catalyst at 1173 K ensured that PdO decomposition was complete and consequently the sintering observed was relevant to the behaviour of Pd^0 rather than PdO. Furthermore, they showed that phase transformation of the Al_2O_3 during hydrothermal aging did not considerably contribute to Pd sintering [16].

Escandón et al. [9] have examined the effect of hydrothermal aging at lower temperatures, where PdO is thermodynamically stable. A significant irreversible decrease in CH_4 conversion over 1 wt.% Pd/ZrO_2–Ce after thermal aging in 2 (v/v)% H_2O/air at 573, 698, and 823 K for 30 h was reported, and the extent of catalyst deactivation increased with aging temperature. The $T_{50\%}$ increased from 648 K for the fresh oxidized catalyst, to 723 K for the air-aged catalyst and >823 K for the hydrothermally aged catalyst. The Pd dispersion and BET surface area of the aged catalysts remained

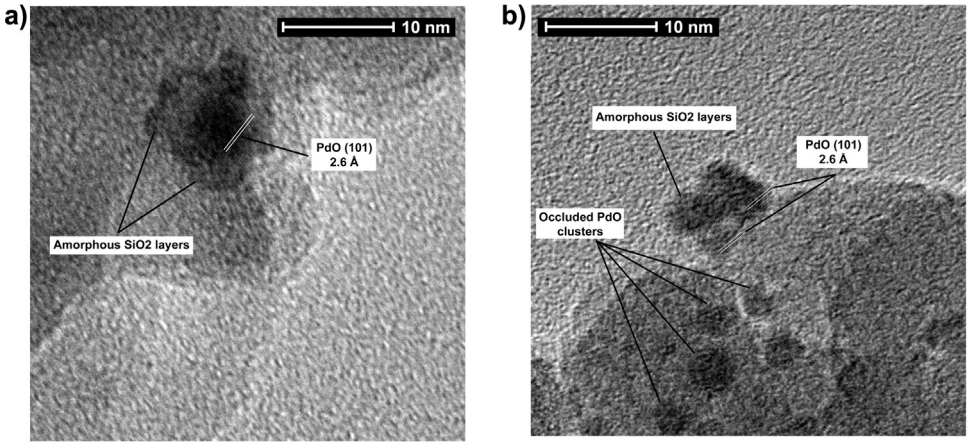

Fig. 9. TEM images of 7.7 wt.% Pd/SiO_2 showing amorphous layers on top of PdO: (a) Catalyst D; (b) Catalyst F. Catalyst identity follows Table 1.

unchanged [9]. The data of Fig. 1 show similar trends, where the largest deactivation of the PdO/SiO_2 catalyst occurred after hydrothermal aging at 973 K ($T_{50\%}$ = 623 K) compared to aging in dry air ($T_{50\%}$ = 544 K). However, the data of Table 1 show that sintering of PdO was inhibited in the presence of the added water, so that the observed activity loss could not be a consequence of PdO cluster size increase alone.

The growth of catalytic particles on SiO_2 supports is complex. According to Hansen et al. [18], the sintering rate of metal nanoparticles depends on their size. For nanoparticles <3 nm in diameter, Ostwald ripening is the most likely sintering mechanism. For larger particles (3–10 nm), both Ostwald ripening and particle migration and coalescence may occur, but the sintering rate is much slower than for the smaller particles [18]. The particle sintering rate has also been shown to correlate with the vapor pressure of the surface species [42]. Pd is unique among the PGMs in that the oxide (PdO) has a much lower vapor pressure than the metal (Pd) [42], and consequently, one would expect a very low sintering rate of PdO by Ostwald ripening [42]. On supported catalysts Ostwald ripening may lead to particles greater in size than the size of the support pores [18]. The data of Tables 1 and 2 show that the PdO size was greater than the SiO_2 support pore size (10–11 nm) only after extended aging in air at 973 K. These data are consistent with a very slow Ostwald ripening of the PdO particles.

The rate of sintering is also known to be dependent on the support. For example, Lamber et al. [43] suggested that on SiO_2 in the presence of water, the formation of silanol (Si–OH) groups favors the migration and coalescence of Pd, whereas in the absence of water, Ostwald ripening is favored. Furthermore, thermal aging of Pd/Al_2O_3 catalysts under lean conditions (16% O_2, 10% CO_2 balance of N_2) at 973 K led to no change in PdO cluster size [44], reflecting the stronger metal-support interaction of Al_2O_3 compared to SiO_2 which limited PdO sintering. The sintering of Pt catalysts on different supports has also been shown to be dependent upon the metal-support interaction [45]. The sintering rate of Pt clusters correlated with electron density of oxygen in the oxide supports during thermal aging in air at 1073 K. As the electron density of oxygen in the support increased ($SiO_2 < Al_2O_3 < ZrO_2 < TiO_2 < CeO_2$) the Pt-oxide-support bond strengthened, which contributed to a decrease in sintering rate [46].

The data reported herein suggest that the SiO_2 also plays a key role in the catalyst deactivation observed in the present study. SiO_2 desorbs physisorbed water at ~370 K whereas chemisorbed water (silanol groups—Si–OH) desorbs at ~670 K [43]. The formation of hydroxides according to the reaction:

$$SiO_{2(s)} + 2H_2O_{(g)} \leftrightarrow Si(OH)_{4(g)} \quad (1)$$

is feasible at temperatures above 973 K [47,48], the hydrothermal aging temperature of the present study. The hydroxyls are expected to change the metal-support interaction [18,43] and decrease the oxygen exchange with PdO sites which are key to high activity [26]. Furthermore, at high temperature, the hydroxyls on the support surface are mobile. Zhu et al. [49] reported the encapsulation of PdO active sites by SiO_2 during CH_4 oxidation at 598 K and during reduction in H_2 at 923 K over a Pd/SiO_2 catalyst. The authors suggested that the high temperature, the H_2O formed during reaction, and the formation of Pd silicide during reduction followed by oxidation in O_2, were all important factors promoting the encapsulation of PdO by the SiO_2. The generation of SiO_2 overlayers on Pd clusters by low temperature H_2 reduction (573 K) has also been reported [50] and the migration of SiO_2 over metal catalysts in systems containing H_2O or H_2 are reported in the literature [43,51,52]. Given the H_2 reduction conditions (673 K) of the present study, the occlusion of Pd clusters even before aging or reaction was therefore likely. HRTEM images and CO uptakes of thermally-aged catalysts from the present study (Fig. 9) show the presence of amorphous layers on top of PdO after thermal aging in air (Catalyst D) or air/water (Catalyst F) and hence, these data do not clarify if the PdO occlusion was exacerbated in the presence of water. The XPS data of Table 1, on the other hand, show that the Pd/Si ratio was significantly lower for the hydrothermally aged PdO/SiO_2 catalyst (Catalyst F) compared to the thermally aged catalyst (Catalyst D), despite smaller PdO particles on the former, and consistent with SiO_2 overlayers reducing PdO growth, but also reducing activity by limiting access to PdO by the gas reactants. These data support the notion that migration of SiO_2 and occlusion of PdO is responsible for the larger deactivation and inhibition by water observed for the hydrothermally aged catalyst compared to the thermally aged catalyst. As shown above, PdO sintering is inhibited significantly by water during thermal aging in air/water versus air. It is expected that the migration of SiO_2 and PdO occlusion establishes a strong metal-support interaction [43,51], which hinders PdO sintering. A similar mechanism of decreased sintering by oxide support overlayers has been demonstrated for Pd and Au catalysts. Several studies have also reported enhanced sintering resistance of Pd catalysts after encapsulation by SiO_2 [53–55] and Au nanoparticles have been stabilized on oxide supports using overlayers of Al_2O_3 [56] and SiO_2 [57] and by TiO_2 modification of a silica support surface [58]. In addition, an increase in the surface area of $Pd@SiO_2$ core–shell catalysts, with porous SiO_2 shells and hence lower mass transfer hindrance for access of reactants to active sites, is believed to enhance catalyst activity, compared to conventional Pd/SiO_2 catalysts [59]. In the present study, the encapsulation appears to also reduce PdO sintering, however, the support loses surface area and porosity and the thickness of the SiO_2 overlayer is not controlled so that the catalyst activity decreases significantly after occlusion. Finally, we note that the CO uptake data of Table 2 suggest that occlusion of smaller PdO particles is more likely than for larger particles, since the CO uptake was lowest for the catalyst with the lowest Pd loading, which is expected to have the smallest PdO particles.

5. Conclusions

PdO/SiO_2 catalysts used for CH_4 oxidation, deactivated when aged in air or air/water at elevated temperatures (723–973 K). Hydrothermal aging of PdO catalysts resulted in a significant irreversible decrease in CH_4 oxidation activity of the catalysts, compared to aging in air at the same temperature. The PdO catalysts sintered during aging in both air and air/water, although the growth and restructuring of the PdO clusters was suppressed by the presence of added water. The higher degree of catalyst deactivation in the presence of air/water compared to air, was mostly due to occlusion of PdO by SiO_2. Amorphous overlayers of SiO_2 on the PdO were confirmed by TEM and XPS analysis. Although hydrothermal aging and H_2-reduction likely both contribute to the PdO occlusion by SiO_2, the XPS data showed a significant increase in PdO occlusion after hydrothermal aging that increased catalyst deactivation and decreased PdO sintering.

Acknowledgements

The financial support of Westport Innovations Inc., Natural Sciences and Engineering Research Council of Canada (NSERC), and the BCFRST Natural Resources and Applied Sciences Program is gratefully acknowledged. The assistance of the Bioimaging Facility at the University of British Columbia for the TEM measurements is also gratefully acknowledged. We also acknowledge the assistance of Dr. Blades's group, Department of Chemistry, UBC for making the Raman measurements.

References

[1] P. Gélin, M. Primet, Appl. Catal. B: Environ. 39 (2002) 1–37, http://dx.doi.org/10.1016/S0926-3373(02)76-0.
[2] T.V. Choudhary, S. Banerjee, V.R. Choudhary, Appl. Catal. A: Gen. 234 (2002) 1–23, http://dx.doi.org/10.1016/S0926-860X(02)231-4.
[3] F.H. Ribeiro, M. Chow, R.A. Dallabetta, J. Catal. 146 (1994) 537–544, http://dx.doi.org/10.1006/jcat.1994.1092.
[4] G. Zhu, J. Han, D.Y. Zemlyanov, F.H. Ribeiro, J. Am. Chem. Soc. 126 (2004) 9896–9897, http://dx.doi.org/10.1021/ja049406s.
[5] T.V. Choudhary, S. Banerjee, V.R. Choudhary, Catal. Commun. 6 (2005) 97–100, http://dx.doi.org/10.1016/j.catcom.2004.11.004.
[6] L.F. Liotta, G. Di Carlo, G. Pantaleo, A.M. Venezia, G. Deganello, E. Merlone Borla, M. Pidria, Appl. Catal. B: Environ. 75 (2007) 182–188, http://dx.doi.org/10.1016/j.apcatb.2007.04.012.
[7] D. Ciuparu, M.R. Lyubovsky, E. Altman, L.D. Pfefferle, A. Datye, Catal. Rev. 44 (2002) 593–649, http://dx.doi.org/10.1081/CR-120015482.
[8] R.F. Hicks, H. Qi, M.L. Young, R.G. Lee, J. Catal. 122 (1990) 280–294, http://dx.doi.org/10.1016/0021-9517(90)90,282-O.
[9] L.S. Escandón, D. Niño, E. Díaz, S. Ordóñez, F.V. Díez, Catal. Commun. 9 (2008) 2291–2296, http://dx.doi.org/10.1016/j.catcom.2008.05.026.
[10] G. Groppi, W. Ibashi, M. Valentini, P. Forzatti, Chem. Eng. Sci. 56 (2001) 831–839, http://dx.doi.org/10.1016/S0009-2509(00)295-5.
[11] G. Corro, C. Cano, J.L.G. Fierro, J. Mol. Catal. A: Chem. 315 (2010) 35–42, http://dx.doi.org/10.1016/j.molcata.2009.08.023.
[12] S. Ordóñez, J.R. Paredes, F.V. Díez, Appl. Catal. A: Gen. 341 (2008) 174–180, http://dx.doi.org/10.1016/j.apcata.2008.02.042.
[13] H. Yoshida, T. Nakajima, Y. Yazawa, T. Hattori, Appl. Catal. B: Environ. 71 (2007) 70–79, http://dx.doi.org/10.1016/j.apcatb.2006.08.010.
[14] C. Lv, K. Ling, G. Wang, J. Chem. Phys. 131 (2009) 144704–144709.
[15] J. Han, D.Y. Zemlyanov, F.H. Ribeiro, Catal. Today 117 (2006) 506–513, http://dx.doi.org/10.1016/j.cattod.2006.06.015.
[16] Q. Xu, K. Kharas, B. Croley, A. Datye, Top. Catal. 55 (2012) 78–83, http://dx.doi.org/10.1007/s11244-012-9770-x.
[17] Q. Xu, K.C. Kharas, B.J. Croley, A.K. Datye, ChemCatChem 3 (2011) 1004–1014, http://dx.doi.org/10.1002/cctc.201000392.
[18] T.W. Hansen, A.T. DeLaRiva, S.R. Challa, A.K. Datye, Acc. Chem. Res. 46 (2013) 1720–1730, http://dx.doi.org/10.1021/ar3002427.
[19] S. Kang, S. Han, S. Nam, I. Nam, B. Cho, C. Kim, S. Oh, Top. Catal. 56 (2013) 298–305, http://dx.doi.org/10.1007/s11244-013-9970-z.
[20] J.G. McCarty, G. Malukhin, D.M. Poojary, A.K. Datye, Q. Xu, J. Phys. Chem. B 109 (2005) 2387–2391, http://dx.doi.org/10.1021/jp048822w.
[21] P. Gélin, L. Urfels, M. Primet, E. Tena, Catal. Today 83 (2003) 45–57, http://dx.doi.org/10.1016/S0920-5861(03)215-3.
[22] K. Persson, L.D. Pfefferle, W. Schwartz, A. Ersson, S.G. Järås, Appl. Catal. B: Environ. 74 (2007) 242–250, http://dx.doi.org/10.1016/j.apcatb.2007.02.015.
[23] W.R. Schwartz, L.D. Pfefferle, J. Phys. Chem. C 116 (2012) 8571–8578, http://dx.doi.org/10.1021/jp2119668.
[24] K. Fujimoto, F.H. Ribeiro, M. Avalos-Borja, E. Iglesia, J. Catal. 179 (1998) 431–442, http://dx.doi.org/10.1006/jcat.1998.2178.
[25] K. Persson, L.D. Pfefferle, W. Schwartz, A. Ersson, S.G. Järås, Appl. Catal. B: Environ. 74 (2007) 242–250, http://dx.doi.org/10.1016/j.apcatb.2007.02.015.
[26] W.R. Schwartz, D. Ciuparu, L.D. Pfefferle, J. Phys. Chem. C 116 (2012) 8587–8593, http://dx.doi.org/10.1021/jp212236e.
[27] R.G. Silver, J.C. Summers, in: A. Freunet, J.M. Bastin (Eds.), Catalysis and Automotive Pollution Control III, Studies in Surface Science and Catalysis, 96, 1995, pp. 871–884.
[28] A. Fathali, L. Olsson, F. Ekström, M. Laurell, B. Andersson, Top. Catal. 56 (2013) 323–328, http://dx.doi.org/10.1007/s11244-013-9974-8.
[29] R.J. Farrauto, M.C. Hobson, T. Kennelly, E.M. Waterman, Appl. Catal. A: Gen. 81 (1992) 227–237, http://dx.doi.org/10.1016/0926-860X(92)80,095-T.
[30] J. Park, J.H. Cho, Y.J. Kim, E.S. Kim, H.S. Han, C. Shin, Appl. Catal. B: Environ. 160–161 (2014) 135–143, http://dx.doi.org/10.1016/j.apcatb.2014.05.013.
[31] F. Sotoodeh, K.J. Smith, J. Catal. 279 (2011) 36–47, http://dx.doi.org/10.1016/j.jcat.2010.12.022.
[32] A.K. Datye, J. Bravo, T.R. Nelson, P. Atanasova, M. Lyubovsky, L. Pfefferle, Appl. Catal. A: Gen. 198 (2000) 179–196, http://dx.doi.org/10.1016/S0926-860X(99)512-8.
[33] K. Otto, C.P. Hubbard, W.H. Weber, G.W. Graham, Appl. Catal. B: Environ. 1 (1992) 317–327, http://dx.doi.org/10.1016/0926-3373(92)80,056-6.
[34] S.C. Su, J.N. Carstens, A.T. Bell, J. Catal. 176 (1998) 125–135, http://dx.doi.org/10.1006/jcat.1998.2028.
[35] A. Baylet, P. Marecot, D. Duprez, P. Castellazzi, G. Groppi, P. Forzatti, Phys. Chem. Chem. Phys. 13 (2011) 4607–4613.
[36] F.P.J.M. Kerkhof, J.A. Moulijn, J. Phys. Chem. 83 (1979) 1612–1619, http://dx.doi.org/10.1021/j100475a011.
[37] R. Burch, F.J. Urbano, P.K. Loader, Appl. Catal. A: Gen. 123 (1995) 173–184, http://dx.doi.org/10.1016/0926-860X(94)251-7.
[38] M. Lyubovsky, L. Pfefferle, A. Datye, J. Bravo, T. Nelson, J. Catal. 187 (1999) 275–284, http://dx.doi.org/10.1006/jcat.1999.2545.
[39] D. Ciuparu, E. Perkins, L. Pfefferle, Appl. Catal. A: Gen. 263 (2004) 145–153, http://dx.doi.org/10.1016/j.apcata.2003.12.006.
[40] D. Ciuparu, N. Katsikis, L. Pfefferle, Appl. Catal. A: Gen. 216 (2001) 209–215, http://dx.doi.org/10.1016/S0926-860X(01)558-0.
[41] P. Araya, S. Guerrero, J. Robertson, F.J. Gracia, Appl. Catal. A: Gen. 283 (2005) 225–233, http://dx.doi.org/10.1016/j.apcata.2005.01.009.
[42] J. Barbier Jr., D. Duprez, Appl. Catal. B: Environ. 4 (1994) 105–140, http://dx.doi.org/10.1016/0926-3373(94)80,046-4.
[43] R. Lamber, N. Jaeger, G. Schulz-Ekloff, J. Catal. 123 (1990) 285–297, http://dx.doi.org/10.1016/0021-9517(90)90,128-7.
[44] X. Chen, Y. Cheng, C.Y. Seo, J.W. Schwank, R.W. McCabe, Appl. Catal. B: Environ. 163 (2015) 499–509, http://dx.doi.org/10.1016/j.apcatb.2014.08.018.
[45] H. Shinjoh, Catal. Surv. Asia 13 (2009) 184–190, http://dx.doi.org/10.1007/s10563-009-9076-6.
[46] Y. Nagai, T. Hirabayashi, K. Dohmae, N. Takagi, T. Minami, H. Shinjoh, S. Matsumoto, J. Catal. 242 (2006) 103–109, http://dx.doi.org/10.1016/j.jcat.2006.06.002.
[47] N.S. Jacobson, E.J. Opila, D.L. Myers, E.H. Copland, J. Chem. Thermodyn. 37 (2005) 1130–1137, http://dx.doi.org/10.1016/j.jct.2005.02.001.
[48] E. Opila, N. Jacobson, D. Myers, E. Copland, JOM 58 (2006) 22–28, http://dx.doi.org/10.1007/s11837-006-0063-3.
[49] G. Zhu, K. Fujimoto, D.Y. Zemlyanov, A.K. Datye, F.H. Ribeiro, J. Catal. 225 (2004) 170–178, http://dx.doi.org/10.1016/j.jcat.2004.03.033.
[50] P.A. Crozier, R. Sharma, A.K. Datye, Microsc. Microanal. 4 (1998) 278–285, http://dx.doi.org/10.1017/S143192769898028X.
[51] C.R.F. Lund, J.A. Dumesic, J. Catal. 72 (1981) 21–30, http://dx.doi.org/10.1016/0021-9517(81)90,074-9.
[52] D.C. Kershner, J.W. Medlin, Surf. Sci. 602 (2008) 786–794, http://dx.doi.org/10.1016/j.susc.2007.12.006.
[53] A.J. Forman, J. Park, W. Tang, Y. Hu, G.D. Stucky, E.W. McFarland, ChemCatChem 2 (2010) 1318–1324, http://dx.doi.org/10.1002/cctc.201000015.
[54] L. Adijanto, D.A. Bennett, C. Chen, A.S. Yu, M. Cargnello, P. Fornasiero, R.J. Gorte, J.M. Vohs, Nano Lett. 13 (2013) 2252–2257, http://dx.doi.org/10.1021/nl4008216.
[55] M. Cargnello, J.J.D. Jaén, J.C.H. Garrido, K. Bakhmutsky, T. Montini, J.J.C. Gámez, R.J. Gorte, P. Fornasiero, Science 337 (2012) 713–717, http://dx.doi.org/10.1126/science.1222887.
[56] J. Lu, B. Fu, M.C. Kung, G. Xiao, J.W. Elam, H.H. Kung, P.C. Stair, Science 335 (2012) 1205–1208, http://dx.doi.org/10.1126/science.1212906.
[57] J. Gabaldon, M. Bore, A. Datye, Top. Catal. 44 (2007) 253–262, http://dx.doi.org/10.1007/s11244-007-0298-4.
[58] S.N. Rashkeev, S. Dai, S.H. Overbury, J. Phys. Chem. C 114 (2010) 2996–3002, http://dx.doi.org/10.1021/jp9091738.
[59] J. Park, A.J. Forman, W. Tang, J. Cheng, Y. Hu, H. Lin, E.W. McFarland, Small 4 (2008) 1694–1697, http://dx.doi.org/10.1002/smll.200800895.